Biochemical and Biophysical Research Communications 423 (2012) 325–330

Contents lists available at SciVerse ScienceDirect

Biochemical and Biophysical Research Communications

journal homepage: www.elsevier.com/locate/ybbrc

Size-controlled nanopores in lipid membranes with stabilizing electric fields

M. Laura Fernández [a,b,c], Marcelo Risk [a,b,c], Ramon Reigada [d], P. Thomas Vernier [e,*]

[a] Laboratorio de Sistemas Complejos, Departamento de Computación, Facultad de Ciencias Exactas y Naturales, Universidad de Buenos Aires, Buenos Aires, Argentina
[b] Consejo Nacional de Investigaciones Científicas y Técnicas, Buenos Aires, Argentina
[c] Area de Bioingeniería, Instituto Tecnológico de Buenos Aires, Buenos Aires, Argentina
[d] Department de Química Física and Institut de Química Teòrica i Computacional (IQTCUB), Universitat de Barcelona, Barcelona, Spain
[e] Ming Hsieh Department of Electrical Engineering, Viterbi School of Engineering, University of Southern California, Los Angeles, CA, USA

ARTICLE INFO

Article history:
Received 21 May 2012
Available online 31 May 2012

Keywords:
Electroporation
Molecular dynamics
Lipid membrane
Stable size-controlled Pores
Electric field

ABSTRACT

Molecular dynamics (MD) has been shown to be a useful tool for unveiling many aspects of pore formation in lipid membranes under the influence of an applied electric field. However, the study of the structure and transport properties of electropores by means of MD has been hampered by difficulties in the maintenance of a stable electropore in the typically small simulated membrane patches. We describe a new simulation scheme in which an initially larger porating field is systematically reduced after pore formation to lower stabilizing values to produce stable, size-controlled electropores, which can then be characterized at the molecular level. A new method allows the three-dimensional modeling of the irregular shape of the pores obtained as well as the quantification of its volume. The size of the pore is a function of the value of the stabilizing field. At lower fields the pore disappears and the membrane recovers its normal shape, although in some cases long-lived, fragmented pores containing unusual lipid orientations in the bilayer are observed.

© 2012 Elsevier Inc. All rights reserved.

1. Introduction

The study of processes that involve the transport of chemical compounds across the plasma membrane into the cell interior is relevant for many techniques used in medicine and biology. The application of an external electric field is the basis for the transfection of genetic material [1] and for drug delivery, including electrochemotherapy for cancer [2,3]. Although the process was initially called electroporation, following the hypothesis that supraphysiological transmembrane electric fields cause the formation of conductive pores in the membrane, the more general term electropermeabilization is also used, to emphasize that a complete molecular mechanism, including the precise structure of the conductive membrane, has not been established. Recently, molecular dynamics (MD) simulations have shown that a transverse electric field can produce pores in phospholipid bilayers [4], and MD has been adopted as a useful method for studying electroporation. A molecular mechanism has been unveiled [4–6], at least for phospholipid bilayers, and the different stages of pore formation have been characterized [7]. However, despite its doubtless utility, MD has a major drawback. The value of the applied field, E, used in the simulations has to be high enough ($E \geqslant E_0$, where E_0 is the minimum field required to electroporate [6,8]) to overcome the large activation energy required to initiate pore formation in a reasonable time window (<100 ns). Under these circumstances the pore formation process can be followed without problem, but the pore expands to the size of the simulated bilayer patch (<100 nm^2 in most all-atom MD simulations of phospholipid bilayers), and strong finite size effects appear. This limitation is an obstacle to the study of the properties and behavior of the long-lasting, quasi-stable pores that are believed to exist in living, electroporated cell membranes on the basis of experimental evidence, including ion conductance [9].

We have developed a two-step protocol based on the observation that the lipid nanopores formed in our simulations can be stabilized by reducing the applied electric field from a higher porating value to a range of lower stabilizing values. Similar stabilized pores have been recently mentioned in electroporation simulations of POPC bilayers [10] and bacterial membranes [11]. Here we describe the first systematic analysis of the dependence of the electropore volume on the strength of the sustaining field. We introduce also a new method for quantifying the volume of the pore, and we show that these stabilized pores can be sustained in bilayers containing cholesterol, an important component of living cell membranes.

First, the pore is initiated by applying a strong electric field, $E_p \geqslant E_0$. Second, when the electropore has expanded [7], the electric field is lowered to a sustaining value $E_s < E_0$. We have observed that for a range of values of E_s, the pore attains a stable size within the simulation box. Moreover, the method is shown to be consistent in the sense that the dimensions of the stabilized pore are

* Corresponding author.
E-mail address: vernier@usc.edu (P.T. Vernier).

0006-291X/$ - see front matter © 2012 Elsevier Inc. All rights reserved.
http://dx.doi.org/10.1016/j.bbrc.2012.05.122

exclusively determined by the final sustaining field E_s and depend neither on the initial porating field nor on the exact time at which the field is reduced. Our procedure provides a tool for studying transport and other properties of stabilized pores of different sizes in MD simulations by modifying the value of the applied field within an appropriate range, which depends on the membrane constituents and on the size of the simulation membrane plane.

The generation of stable and size-controlled electropores following the strategy mentioned above has been validated in simulations of fully hydrated dioleoylphosphatidylcholine (DOPC) bilayers containing up to 40 mol% of cholesterol (Chol) (see Section 2.1). Cholesterol is the most common lipid component in animal cell membranes (up to 0.4 molar fraction) [12] and is a key determinant of membrane physical properties, so cholesterol-containing bilayers are an important component of the set of models for biological membranes. Similar qualitative results are observed for a range of Chol fractions and for bilayers which do not contain Chol (not shown).

We have characterized these size-controlled, stable nanopores by means of a new geometric method for quantifying the volume of the nanopores. Using MD simulations the behavior of these structures is analyzed, and a range of electric fields that lead to stable pores is obtained. In Section 2, the simulation protocols are presented as well as the method for pore volume calculation. Evolution of the pore volume in pore-stabilizing electric fields, pore stabilization, pore annihilation and restructuring of the bilayer, and the appearance of fragmented pores are discussed in Section 3.

2. Methods

2.1. Computational methods

We performed simulations of phospholipid bilayer systems composed of DOPC and 40% mol of cholesterol, corresponding to a composition of 128 DOPC and 86 cholesterol molecules distributed randomly in the two leaflets. All systems were hydrated with 6186 water molecules. The systems were prepared as described in our previous work in Ref. [8]. Simulations were carried out using the GROMACS 3.3.1 software package [13].

For DOPC molecules we used the standard united-atom forcefield parameters developed by Berger et al. [14]. Partial charges were taken from Ref. [15], and the force field parameters for the double-bond region are based on the adaptation performed by Bachar et al. [16,17]. The Simple Point Charge (SPC) model [18] was employed for water. The force field parameters of Holtje et al. [19] were adapted for cholesterol. The SETTLE algorithm [20] was used to preserve the bond lengths in water molecules, and lipid bond lengths were constrained with the LINCS algorithm [21]. A single 1.0 nm cut-off distance was used for Lennard-Jones interactions. Long-range electrostatic interactions were handled using the particle-mesh Ewald method [22] with a real space cut-off of 1.0 nm, β-spline interpolation (of order 6), and direct sum tolerance of 10^{-5}. Periodic boundary conditions were used in all three directions, and the time step was set to 2 fs.

Simulations were carried out in the NpT ensemble at $p = 1$ atm and $T = 310$ K. Temperature and pressure were controlled by using the weak coupling method [23] with relaxation times set to 0.6 and 1.0 ps, respectively. The pressure coupling was applied separately in the bilayer plane (x,y) and the perpendicular direction (z). Membranes were equilibrated for 10 ns at 310 K before the electric field was applied. Equilibration of bilayers was determined by monitoring the membrane area until a stable area per lipid was achieved. Once equilibrated, membranes are subjected to an electric field, E, in the direction normal to the membrane (x,y) plane. It is worth noting here that caution must be exercised when comparing the applied fields in MD simulations with real field values in electroporation experiments. In the laboratory, the electric field is taken as the potential difference between electrodes divided by the distance separating them, and this corresponds to the sum of the field due to the free charge at the electrodes and the polarization of fixed charges in the system. In contrast, the applied field in MD simulations corresponds only to the field generated from the charges at the electrodes without considering the electric response of the medium. Here, we have chosen this simulated external applied field as a control parameter.

The simulation protocol applied here has been successfully applied in previous MD simulations [24,25], and the obtained values for structural membrane properties, in the absence of an external electric field, such as the area per molecule, the membrane thickness, and the scattering form factors are consistent with experimental data for DOPC and DOPC/Chol bilayers. Molecular visualization was performed using Visual Molecular Dynamics, VMD [26]. The analysis of the simulation trajectories was performed using custom programs, developed in Python [27]. Statistical analysis of the obtained properties was carried out in the R environment [28].

2.2. Generation of stable nanopores

After equilibration of the bilayer system (see Section 2.1), a transverse electric field of 750 mV/nm was applied. This value of the applied field corresponds to the minimum electroporating field, E_0, computed in our previous work [8], so that after a few nanoseconds a pore is generated. The initial stages of pore growth were followed by monitoring the number of phosphorus atom groups that reside in the internal nonpolar region (Fig. 1A). Once this number exceeds a (arbitrary) value of 18, visual inspection of the membrane reveals that the phosphorous groups initially belonging to the two leaflets have merged into a common phosphorous group, indicating that a hydrophilic pore has formed [7]. At this point, the simulation was stopped, and the geometry of the pore was recorded. Using this stage as a starting point, we continued the simulation, but now with various lower values for the electric field: 0 (no field), 50, 75, 100, 125, 150, 175, 200, 250, and 300 mV/nm. Each case was run independently up to 100 ns in triplicate.

2.3. Nanopore volume measurement

In each simulation, the temporal evolution of the structure of the pores was monitored. To accurately characterize the pore geometry at a given time, a three-step algorithm is applied. First, the pore has to be centered inside the simulation box (a rectangular cuboid of approximately 7.5 nm for each side). The centering algorithm looks for the center of mass of the membrane and applies an offset in order to place the center of mass of the membrane at the center of the simulation box. Second, once the pore has been centered, the membrane is partitioned in three different parts: the upper polar region, the internal nonpolar region, and the lower polar region (Fig. 1A). In order to detect the borders of the internal nonpolar region in the z direction, the average position of the z coordinate is computed for the first methylene carbon of the *sn-1* acyl chains of DOPC molecules not implicated in the pore. The average z position of the first methylene *sn-1* groups, Z_{up} and Z_{down}, and the corresponding standard deviation, SD_{up} and SD_{down}, were calculated for the upper and the lower leaflets, respectively. The nonpolar region is then considered to be confined between ($Z_{down} + 2\ SD_{down}$ and $Z_{up} + 2\ SD_{up}$). Third, the system volume occupied by water molecules in the pore is sliced in cylindroids (cylinder with elliptical base in the x,y plane) with a height of

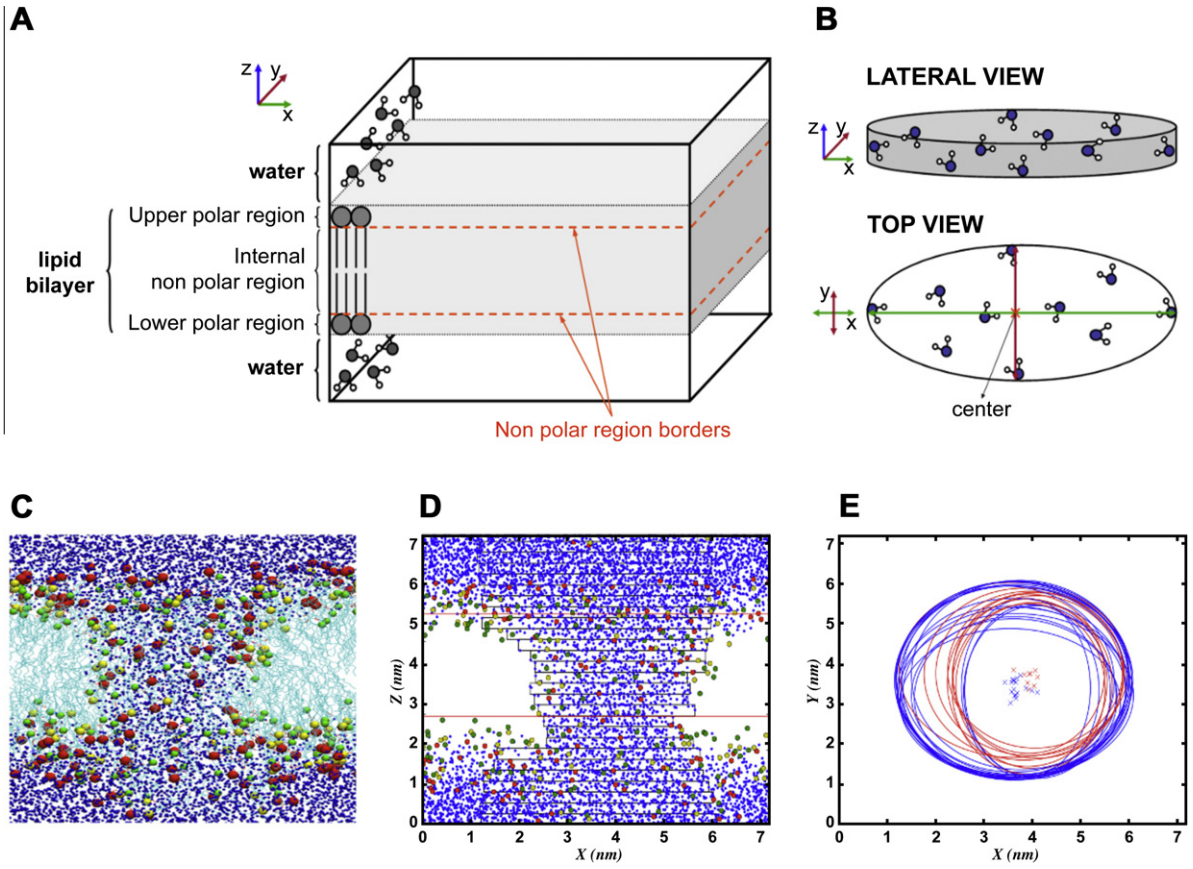

Fig. 1. Schematic representation of (A) the simulation box, indicating the water region, the upper and the lower polar regions of the bilayer and the internal nonpolar region of the bilayer and (B) the cylindroids that constitute the pore (lateral and top view). (C) Snapshot of the initial pore structure. (D) Plot of the (x, z) view of the cylindroids that form the starting pore. Blue spheres are water oxygen atoms, red spheres are the phosphorus atoms of DOPC, yellow spheres are the hydroxyl oxygen atoms of cholesterol, and green spheres are the first *sn-1* carbon atoms of DOPC. (E) Plot of the (x, y) view of the cylindroids that characterize the water pore. Crosses correspond to the center of the cylindroids. The cylindroids of the nonpolar region that contribute to the pore volume are in red; the 'external' cylindroids excluded from the calculation are in blue. (For interpretation of the references to color in this figure legend, the reader is referred to the web version of this article.)

0.15 nm (approximate radius of a water molecule) in the z direction. The radii of the cylindroids are determined taking into account the distances between the most distant water molecules in x and y directions (Fig. 1B), as far as a distance of 5 nm. The volume of the pore, V, is finally geometrically defined and computed as the volume of the geometric figure combining all the cylindroids inside the nonpolar region of the membrane. As an example of the proposed characterization procedure, Fig. 1C, D and E show its application to the initial hydrophilic pore before the electric field is reduced.

3. Results and discussion

Analysis of the simulations with a reduced applied electric field, E_s, reveals three different behaviors. Large values of $E_s \geqslant 200$ mV/nm lead to a progressive increase of the pore volume up to the size of the simulation box. At this point strong finite size effects appear, and the bilayer configuration is lost. At low electric fields, $E_s \leqslant 100$ mV/nm, the pore decreases in volume and eventually disappears, similar to what is observed if the electric field is completely removed [7], and the membrane recovers its compact bilayer conformation.

We note here some interesting variants on the lower field results. Although pore creation and annihilation can be described in a sequence that is applicable to lipid bilayer systems in general [7], each individual pore construction and destruction event is unique, thus more than one or two simulations must be run to find the typical case, and one must also be alert to the significance of instances that do not follow the normal pattern. A few replicas (3 out of the 12 simulations for $E_s \leqslant 100$ mV/nm) did not form a fully repaired bilayer after removal of the field. Instead, during the pore deconstruction process some lipid molecules became trapped in energetically unfavorable orientations, as shown in Fig. 2, where both structures remain at least up to 100 ns under low electric fields or even in the absence of electric field. These "trapped" or "frustrated" configurations include DOPC molecules displaying an inverted orientation (with respect to the others in the same leaflet) and Chol molecules positioned 'horizontally' (tangential to the membrane plane) midway between the two leaflets. In both situations the pore has almost completely disappeared, but a small hydrophilic region remains in the bilayer interior. A few water molecules surround this area, and a close inspection of their dynamics reveals that water is slowly but constantly leaking through these regions of the membrane. To investigate the stability of these leaky, partially decomposed pores we extended some simulations in the absence of any electric field (Fig. 2) and found that the structures remained several tens of nanoseconds, so they can be considered long-lived at least on the time scales of our MD systems.

A more detailed and systematic study of these structures is beyond the scope of this paper and will be presented elsewhere. However, we suggest that the existence of these leaky, fragmented pores is consistent with and may help to explain the long-lived permeabilized state of membranes reported in studies of electro-

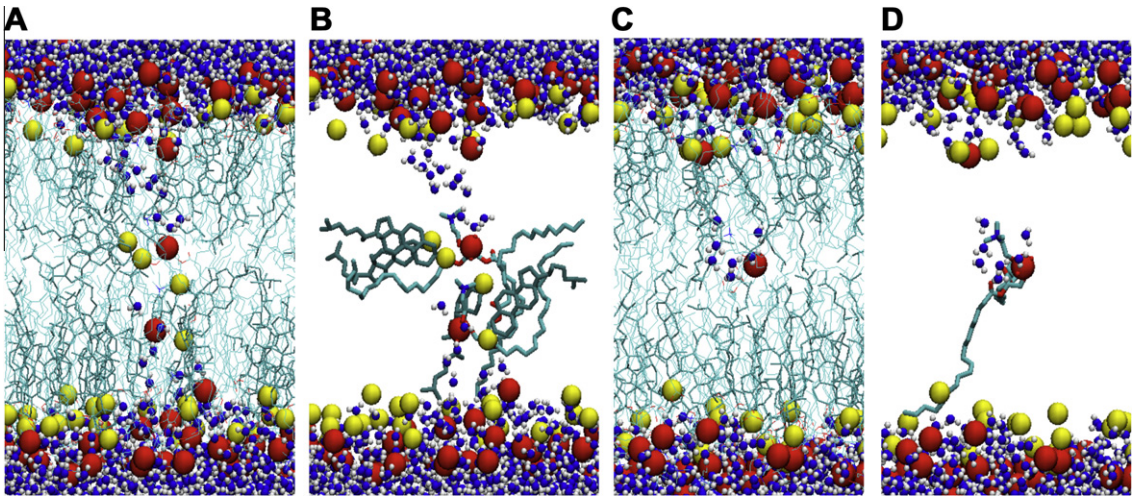

Fig. 2. (A) Snapshot of a trapped configuration obtained at 100 mV/nm. Blue spheres are water oxygen atoms; red spheres are the phosphorus atoms of DOPC; yellow spheres are the hydroxyl oxygen atoms of cholesterol (Chol). Green stick structures are Chol; turquoise stick structures are the lipid hydrocarbon tails. Water molecules are the small blue (oxygen) and gray (hydrogen) spheres. (B) Same as (A), where tails of the DOPC molecules and Chol molecules that form part of the fragmented pore are shown. This configuration is maintained for at least 100 ns after removing the electric field. (C) Snapshot of a trapped DOPC structure from a system sustained at 75 mV/nm. (D) Same frame as (C), showing the DOPC molecule trapped in the middle of the membrane. (For interpretation of the references to color in this figure legend, the reader is referred to the web version of this article.)

poration [9]. We note that cholesterol is a component of the bilayers exhibiting this behavior, suggesting that cholesterol-specific interactions may be responsible for the persistence of these configurations, since they have not been observed by us or reported by others in cholesterol-free systems.

In this paper, we focus on the behavior that is found during application of the intermediate fields, E_s = 125, 150, and 175 mV/nm. In these cases the pore reaches a steady state and displays a stable structure and volume. In Fig. 3, stabilized pores at these three values for the sustaining electric field are plotted, and the corresponding characterizations based on cylindroids are presented.

The temporal behavior of the pore volume, $V(t)$, for one of the three replicas from simulations at each of the three values (125, 150, 175 mV/nm) for sustaining electric field, E_s, is plotted in Fig. 4. The temporal decay of pore volume obtained for E_s < 200 mV/nm can be fitted to an exponential form, $V(t) = a\, e^{-t/\tau} + b$, where b stands for the final estimated volume of the stable pore, and τ corresponds to the time constant of the exponential decay. Table 1 shows the parameters of the exponential fit a, τ and b, for each electric field E_s. Note that the volume of the stabilized pore increases with the value of the sustaining electric field, and that the time constant is relatively independent of electric field, except at the highest value.

In order to show that the strategy provides a general method for obtaining stable pores of controllable size in MD simulations, we performed several tests (data not shown) to assure that the steady-state pore size depends neither on the initial initiating field nor on the exact time the field was reduced, provided that a hydrophilic pore has been formed and that the field is reduced

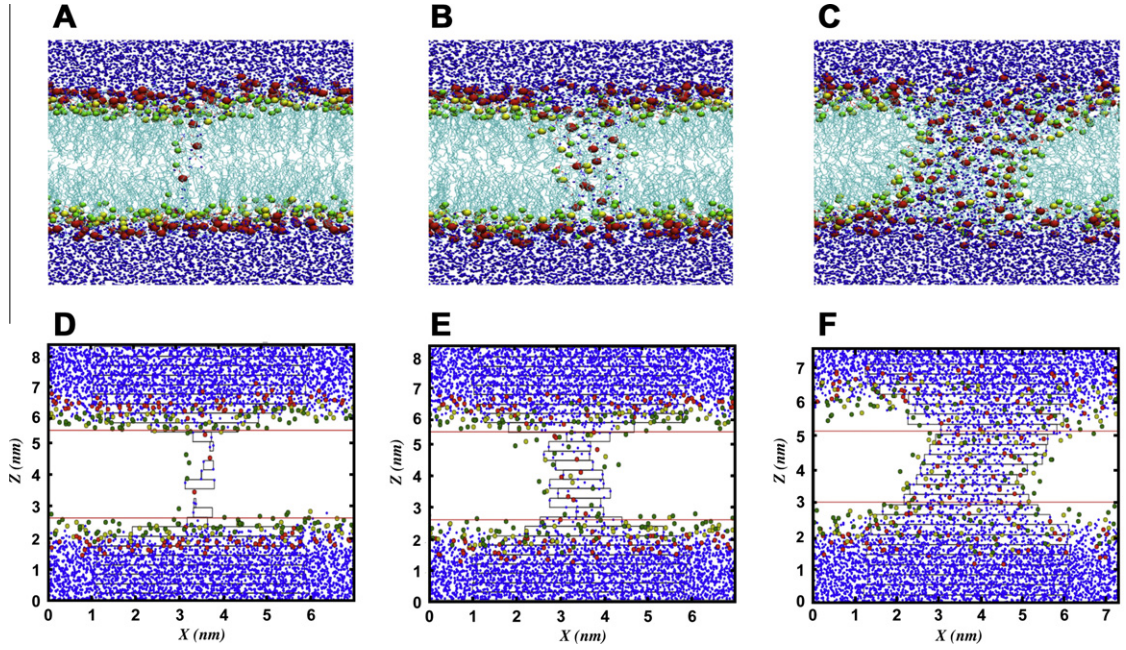

Fig. 3. Snapshots for the stabilized pore structures after 100 ns at (A) E_s = 125 mV/nm, (B) E_s = 150 mV/nm and (C) E_s = 175 mV/nm. The color code in Fig. 2a is used here. (D–F) Plots of the (x,z) view of the cylindroids that form the stabilized pores. The color code in Fig. 2b is used here.

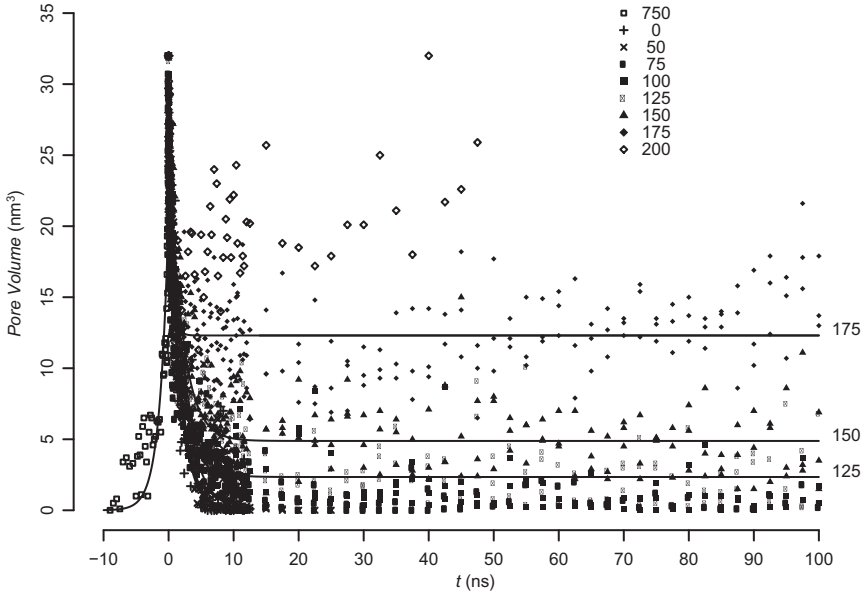

Fig. 4. Estimated pore volume versus time for the opening of the pore with E_p = 750 mV/nm and the subsequent pore evolution upon applying different sustaining fields E_s: 0, 50, 75, 100, 125, 150, 175, and 200 mV/nm. Solid lines correspond to the mean value of the volume at the indicated E_s for times t > 12 ns, when the pores have stabilized.

Table 1
Parameters obtained from the exponential fit, $V(t) = a\ e^{-t/\tau} + b$, for the pore volume V obtained in MD simulations at different reduced electric fields*.

E (mV/nm)	a (nm^3)	a Lower 95% CI (nm^3)	a Upper 95% CI (nm^3)	τ (ns^{-1})	τ Lower 95% CI (ns^{-1})	τ Upper 95% CI (ns^{-1})	b (nm^3)	b Lower 95% CI (nm^3)	b Upper 95% CI (nm^3)
0	25.6	24.8	26.5	1.64	1.47	1.8	na	na	na
50	25.0	24.1	25.9	1.72	1.53	1.92	na	na	na
75	25.4	24.5	26.3	1.79	1.59	1.99	na	na	na
100	24.3	23.5	25.1	2.3	2.07	2.52	na	na	na
125	24.4	23.5	25.2	2.03	1.81	2.24	2.34	1.97	2.71
150	21.2	20.4	22.0	2.07	1.84	2.31	4.88	4.45	5.32
175	17.1	15.8	18.5	0.50	-0.42	1.42	12.31	11.75	12.87

* Mean values and their corresponding 95% confidence intervals (CI), were calculated from three replicas for each E. The CI were obtained by weighting the standard error (standard deviation over square root of the sample size) with the quantile 0.975, and adding and subtracting this error to and from the mean to give the upper and lower limits, respectively. na: not applicable.

before finite size effects appear. Moreover, two simulations were performed taking as starting geometries stable pores at E_s = 125 mV/nm and 175 mV/nm and applying to them fields of 175 mV/nm and 125 mV/nm, respectively. In both cases, the pore adapted to the new electric field and displayed the corresponding sizes within the statistical ranges presented in Table 1. Thus it is clear that the proposed strategy is consistent in the sense that the size of a pore can be determined by modulating the electric field after pore formation. Interestingly, stable pore formation is a process with two electric field thresholds. First, as was demonstrated in our previous work [6–8], the initial stages of pore formation require a porating field, E_p, to overcome the high activation energy for the generation of the intermediate hydrophobic pore (water bridge) and the subsequent lipid rearrangement to form the hydrophilic pore structure. Once the pore has been initiated and begins to expand, a second (lower) threshold for the electric field, $E_{min} < E_p$, must be applied to maintain the hydrophilic pore in a quasi-steady-state structure. Values for both the porating threshold field E_0 and the lower threshold E_{min} depend on the properties of the specific membrane. For example, we have observed how a lower content of Chol in the membrane reduced its cohesion, and this decreases both thresholds, E_0 and E_{min}.

We have shown that nanoscale pores can be formed and then maintained in a quasi-stable state by the application of appropriate electric fields in MD simulations. A systematic analysis of the volume of these nanoscale lipid electropores shows that the size of the pore is a function of the value of the stabilizing electric field. These stabilized electropores can be used for electrical and physical characterization of the properties of lipid nanopores, and will be a tool for continuing investigations of model systems of electropermeabilized membranes.

We have also reported the existence of long-lived pore fragments in some simulations, where a few phospholipid molecules and associated waters remain "trapped" in the middle of the bilayer after the membrane-spanning hydrophilic pore structure has collapsed, in some cases even 100 ns after electric field removal. These remnants of lipid bilayer poration may be related to the structures responsible for the long-lasting permeabilized state observed experimentally in living cell membranes.

Acknowledgments

Computational resources were provided by the Barcelona Supercomputing Center and by the Centro de Cómputos de Alto Rendimiento (CeCAR) – Facultad de Ciencias Exactas y Naturales – UBA. RR acknowledges financial support provided by SEID through project BFU2010-21847-C02-02, by DURSI through project 2009-SGR-1055. PTV was supported in part by the Air Force Office of Scientific Research. MLF and MR were supported by Grants from Universidad de Buenos Aires (UBACyT X132/08), CONICET

(PIP 112-200801-01080/09), and MINCyT (SLO-AR 08/02/09), and MR received additional support from IBM of Argentina. MLF and MR gratefully acknowledge the guidance of Professor G. Marshall.

References

[1] E. Neumann, S. Kakorin, K. Toensing, Fundamentals of electroporative delivery of drugs and genes, Bioelectrochem. Bioenerg. 48 (1999) 3–16.
[2] T.Y. Tsong, Electroporation of cell membranes, Biophys. J. 60 (1991) 297–306.
[3] M. Belehradek, C. Domenge, B. Luboinski, S. Orlowski, J. Belehradek, L.M. Mir, Electrochemotherapy, a new antitumor treatment, Cancer 72 (1993) 3694–3700.
[4] D.P. Tieleman, The molecular basis of electroporation, BMC Biochem. 5 (2004) 10.
[5] M. Tarek, Membrane electroporation: a molecular dynamics study, Biophys. J. 88 (2005) 4045–4053.
[6] M.J. Ziegler, P.T. Vernier, Interface water dynamics and porating electric fields for phospholipid bilayers, J. Phys. Chem. B 112 (2008) 13588–13596.
[7] Z.A. Levine, P.T. Vernier, Life cycle of an electropore: field-dependent and field-independent steps in pore creation and annihilation, J. Membr. Biol. 236 (2010) 27–36.
[8] M.L. Fernández, G. Marshall, F. Sagués, R. Reigada, Structural and kinetic molecular dynamics study of electroporation in colesterol-containing bilayers, J. Phys. Chem. B 114 (2010) 6855–6865.
[9] A.G. Pakhomov, J.F. Kolb, J.A. White, R.P. Joshi, S. Xiao, K.H. Schoenbach, Long-lasting plasma membrane permeabilization in mammalian cells by nanosecond pulsed electric field (nsPEF), Bioelectromagnetics 28 (2007) 655–663.
[10] R.A. Böckmann, B.L. de Groot, S. Kakorin, E. Neumann, H. Grubmüller, Kinetics, statistics, and energetics of lipid membrane electroporation studied by molecular dynamics simulations, Biophys. J. 95 (2008) 1837–1850.
[11] T.J. Piggot, D.A. Holdbrook, S. Khalid, Electroporation of the *E. coli* and *S. Aureus* membranes: molecular dynamics simulations of complex bacterial membranes, J. Phys. Chem. B. 115 (2011) 13381–13388.
[12] H. Ohvo-Rekilä, B. Ramstedt, P. Leppimäki, J.P. Slotte, Cholesterol interactions with phospholipids in membranes, Prog. Lipid Res. 41 (2002) 66–97.
[13] E. Lindahl, B. Hess, D. van der Spoel, GROMACS 3.0: a package for molecular simulation and trajectory analysis, J. Mol. Model. 7 (2001) 306–317.
[14] O. Berger, O. Edholm, F. Jahnig, Molecular dynamics simulations of a fluid bilayer of dipalmitoylphosphatidylcholine at full hydration, constant pressure, and constant temperature, Biophys. J. 72 (1997) 2002–2013.
[15] D.P. Tieleman, H.J.C. Berendsen, Molecular dynamics simulations of a fully hydrated dipalmitoylphosphatidylcholine bilayer with different macroscopic boundary conditions and parameters, J. Chem. Phys. 105 (1996) 4871–4880.
[16] M. Bachar, P. Brunelle, D.P. Tieleman, A. Rauk, Molecular dynamics simulation of a polyunsaturated lipid bilayer susceptible to lipid peroxidation, J. Phys. Chem. B 108 (2004) 7170–7179.
[17] H. Martinez-Seara, T. Róg, M. Karttunen, R. Reigada, I. Vattulainen, Influence of cis double-bond parametrization on lipid membrane properties: how seemingly insignificant details in force-field change even qualitative trends, J. Chem. Phys. 129 (2008) 105103.
[18] H.J.C. Berendsen, J.P.M. Postma, W.F. van Gunsteren, J. Hermans, Interaction models for water in relation to protein hydration, in: B. Pullman (Ed.), Intermolecular Forces, Reidel, Dordrecht, The Netherlands, 1981, pp. 331–342.
[19] M. Holtje, T. Forster, B. Brandt, T. Engels, W. von Rybinski, H.-D. Holtje, Molecular dynamics simulations of stratum corneum lipid models: fatty acids and cholesterol, Biochim. Biophys. Acta 1511 (2001) 156–167.
[20] S. Miyamoto, P.A. Kollman, SETTLE: an analytical version of the SHAKE and RATTLE algorithms for rigid water models, J. Comp. Chem. 13 (1992) 952–962.
[21] B. Hess, H. Bekker, H.J.C. Berendsen, J.G.E.M. Fraaije, LINCS: a linear constraint solver for molecular simulations, J. Comput. Chem. 18 (1997) 1463–1472.
[22] U. Essman, L. Perera, M.L. Berkowitz, H.L.T. Darden, L.G.A Pedersen, smooth particle mesh Ewald method, J. Chem. Phys. 103 (1995) 8577–8592.
[23] H.J.C. Berendsen, J.P.M. Postma, W.F. van Gunsteren, A. DiNola, J.R. Haak, Molecular dynamics with coupling to an external bath, J. Chem. Phys. 81 (1984) 3684–3690.
[24] H. Martinez-Seara, T. Róg, M. Pasenkiewicz-Gierula, I. Vattulainen, M. Karttunen, R. Reigada, Effect of double bond position on lipid bilayer properties: insight through atomistic simulations, J. Phys. Chem. B. 111 (2007) 11162–11168.
[25] H. Martinez-Seara, T. Róg, M. Pasenkiewicz-Gierula, I. Vattulainen, M. Karttunen, R. Reigada, Interplay of unsaturated phospholipids and cholesterol in membranes: effect of the double-bond position, Biophys. J. 95 (2008) 3295–3305.
[26] W. Humphrey, A. Dalke, K. Schulten, VMD – Visual Molecular Dynamics. J. Molec. Graphics. 14 (1996) 33–38. <http://www.ks.uiuc.edu/Research/vmd/>.
[27] <http://www.python.org>
[28] R Development Core Team, R: A Language and Environment for Statistical Computing, R Foundation for Statistical Computing, Vienna, Austria 2011, ISBN 3-900051-07-0.